Detecting diffusion-diffraction patterns in size distribution phantoms using double-pulsed field gradient NMR: Theory and experiments

Noam Shemesh,[1] Evren Özarslan,[2] Peter J. Basser,[2] and Yoram Cohen[1,a)]
[1]*School of Chemistry, The Raymond and Beverly Sackler Faculty of Exact Sciences, Tel Aviv University, Tel Aviv 69778, Israel*
[2]*Section on Tissue Biophysics and Biomimetics, NICHD, National Institutes of Health, Bethesda, Maryland, 20892 USA*

(Received 6 October 2009; accepted 15 December 2009; published online 21 January 2010)

NMR observable nuclei undergoing restricted diffusion within confining pores are important reporters for microstructural features of porous media including, inter-alia, biological tissues, emulsions and rocks. Diffusion NMR, and especially the single-pulsed field gradient (s-PFG) methodology, is one of the most important noninvasive tools for studying such opaque samples, enabling extraction of important microstructural information from diffusion-diffraction phenomena. However, when the pores are not monodisperse and are characterized by a size distribution, the diffusion-diffraction patterns disappear from the signal decay, and the relevant microstructural information is mostly lost. A recent theoretical study predicted that the diffusion-diffraction patterns in double-PFG (d-PFG) experiments have unique characteristics, such as zero-crossings, that make them more robust with respect to size distributions. In this study, we theoretically compared the signal decay arising from diffusion in isolated cylindrical pores characterized by lognormal size distributions in both s-PFG and d-PFG methodologies using a recently presented general framework for treating diffusion in NMR experiments. We showed the gradual loss of diffusion-diffraction patterns in broadening size distributions in s-PFG and the robustness of the zero-crossings in d-PFG even for very large standard deviations of the size distribution. We then performed s-PFG and d-PFG experiments on well-controlled size distribution phantoms in which the ground-truth is well-known *a priori*. We showed that the microstructural information, as manifested in the diffusion-diffraction patterns, is lost in the s-PFG experiments, whereas in d-PFG experiments the zero-crossings of the signal persist from which relevant microstructural information can be extracted. This study provides a proof of concept that d-PFG may be useful in obtaining important microstructural features in samples characterized by size distributions. © *2010 American Institute of Physics*. [doi:10.1063/1.3285299]

I. INTRODUCTION

Accurately characterizing opaque fluid-filled porous samples is important in a multitude of scientific areas ranging from material science to chemistry, biology, and medicine.[1–8] Magnetic resonance (MR) based techniques are among the most important methodologies for probing porous media, owing to their noninvasive and nonperturbing nature. Several valuable properties can be quantified to obtain valuable information about the pores.

Diffusion of NMR observable nuclei within the constituent pores can be used to report on geometrical features of the sample since diffusion is acutely modulated by the surrounding environment. Techniques often used such as diffusion tensor imaging[9] can characterize the anisotropy present when pores are coherently placed within the specimen,[10] while multiple diffusion time experiments can, to a certain extent, characterize the tortuosity and surface to volume ratio[5,11,12] and fractal dimensions[13] of the specimen. Other diffusion-based methods exist to quantify flow phenomena,[14–17] the internal magnetic field of the samples,[18–20] and to a certain extent, exchange properties[21,22] of the porous media. The q-space approach[1,23] introduced yet another important quantifiable microstructural parameter which characterizes the pores: their average size, which is important in most diffusion NMR applications such as emulsions[24] and central nervous system tissues.[1]

Single-pulsed field gradient (s-PFG) methods are conventionally employed to extract the self-diffusion coefficient D of the diffusing moiety.[25] The single-pulsed gradient spin echo (s-PGSE) method incorporates a pair of diffusion sensitizing gradients separated by a diffusion period Δ overlaid on a Hahn spin echo sequence. In the case of free Gaussian diffusion, and when the spins are not confined to any restricting geometry, the diffusion NMR signal ($S(\mathbf{q})$) decays according to

$$E(\mathbf{q}) = e^{-4\pi^2|\mathbf{q}|^2 t_d D}, \tag{1}$$

where $E(\mathbf{q})$ is the normalized signal decay, i.e., $E(\mathbf{q}) = S(\mathbf{q})/S(\mathbf{q}=0)$, and $\mathbf{q}$ is the wave vector defined as $\mathbf{q} = (2\pi)^{-1}\gamma\delta\mathbf{G}$, γ is the gyromagnetic ratio, δ is the duration of the gradient, $\mathbf{G}$ is the gradient vector, t_d is the effective

a)Author to whom correspondence should be addressed. Tel./FAX: 972 3 6407232/972 3 6407469. Electronic mail: ycohen@post.tau.ac.il.

diffusion period ($t_d=\Delta-\delta/3$) in the case of rectangular gradient waveforms), and D is the diffusion coefficient.

In porous media, barriers that hamper the diffusion process are introduced to the sample, and the signal attenuation can no longer be characterized by Eq. (1); therefore, only an apparent diffusion coefficient (ADC) can be extracted. By varying the diffusion period, the ADC can be used to probe the sample at different length scales, and can report on certain microstructural features of the sample.[3,12]

Highly ordered, coherently placed monodisperse pores exhibit the diffusion-diffraction phenomena when E(q) is plotted against the magnitude of the wave vector q, and the diffusion period is sufficiently long to probe the boundaries of the pores.[26,27] These diffusion-diffraction patterns are extremely informative since the diffusion-diffraction troughs resolve important structural information characterizing the sample that is not accessible by other means. The compartment dimension, an important attribute of porous media, can be extracted from the reciprocal of the diffusion-diffraction minima,[26,27] and the high sensitivity of these minima to the orientation of the fiber can be used to obtain the directionality of coherently placed anisotropic pores.[28] Originally observed by Callaghan *et al.*[26] almost 2 decades ago, the theoretical framework for the phenomenon has been established over the years for important geometries and in some cases surface relaxation was incorporated into the theory.[29,30] To establish the accuracy of the structural parameters extracted from these diffusion-diffraction patterns, the effect of numerous experimental parameters has been experimentally tested and theoretically realized on well-controlled systems.[28,30–34] The diffusion-diffraction phenomenon was used to accurately characterize monodisperse systems of micron dimensions such as narrowly distributed emulsions,[35,36] water filled microcapillaries,[28,31–33] red blood cells (RBCs),[37] and even solvent diffusing in polymer cavities.[38]

The diffusion-diffraction patterns may be an extremely powerful means to probe structural information; however, the diffusion-diffraction minima are extremely sensitive to size distributions, and are rapidly lost when the pores in the porous media are characterized by a size distribution.[39,40] This major *caveat* is probably why diffusion-diffractions are not observed in most diffusion NMR studies of neuronal tissue,[1,41,42] broadly distributed emulsions,[43–46] and other porous media which are characterized by a relatively broad size distribution. In fact, in a recent work, Pages *et al.*[47] showed the reversible loss of diffusion-diffraction minima when RBCs transformed from discocytes (relatively monodispere) to spherocytes (broader size distribution). The disappearance of the diffusion-diffraction troughs in porous media characterized by size distributions poses a limitation for the methodology, since it prevents extraction of microstructural information directly from the E(q) plots. When the size distribution is introduced, the signal decay, plotted as a function of the b-value (where $b=4\pi^2|\mathbf{q}^2|t_d$) becomes nonmonoexponential,[48] and is often modeled by a biexponential decay. Although sophisticated methods have been proposed to reconstruct the structural information in samples characterized by size distributions,[24,43,44,49,50] it would be very desirable to infer such information directly from the E(**q**) plots.

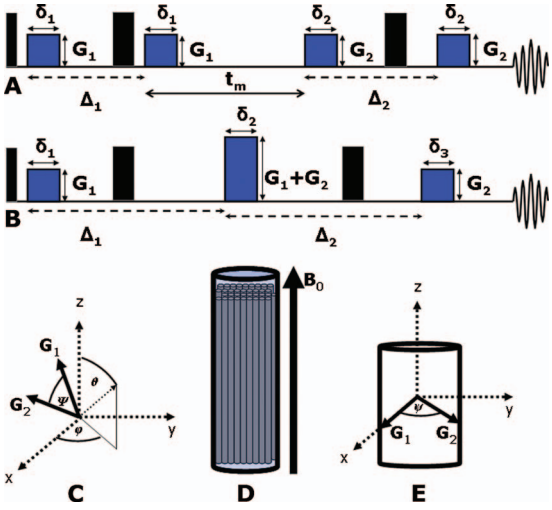

FIG. 1. Sequences and orientation schemes. (a) The d-PFG sequence in which the first and second gradient pairs are separated by a mixing time (t_m). The gradient amplitudes and directions are defined by $\mathbf{G_1}$ and $\mathbf{G_2}$; the gradient durations are defined by δ_1 and δ_2. The first and second diffusion periods are defined by Δ_1 and Δ_2, respectively. (b) The d-PFG sequence in which the second and third gradients are superimposed. In this case, the mixing time is inherently zero and the gradient durations for the first, second, and third gradients are defined as δ_1, δ_2, and δ_3, respectively. In (a) and (b), narrow and wide black boxes represent $\pi/2$ and π pulses, respectively. (c) The angle ψ is defined as the angle between the wave vectors $\mathbf{G_1}$ and $\mathbf{G_2}$. The angles φ and θ are the azimuthal and polar angles, respectively. (d) The phantoms consisted of water filled microcapillaries, which were packed in a 4 mm glass sleeve and inserted into a 5 mm NMR tube (not shown) aligned with the main magnetic field. Microcapillaries were counted to comprise the correct volumetric ratio assigned to each phantom. (e) In the angular dependence experiments referred to in this study, $\mathbf{G_1}$ was fixed along the x-direction, while the angle between the gradients, ψ, was varied. In these experiments, ψ was varied in the X-Y plane, i.e., $\theta=90°$ and the orientation of $\mathbf{G_2}$ was varied along the angle φ.

The double-PFG (d-PFG) method, first proposed by Cory *et al.*[51] in 1990, and initially used for flow-related phenomena,[52] suppression of convection artifacts,[53] and two-dimensional diffusion-diffusion correlation spectroscopy,[54] has lately gained increasing attention due to its apparent ability to recover microstructural information that is inherently lost or absent in s-PFG methods such as microscopic anisotropy in macroscopically isotropic samples.[51,55–57] The double-pulsed gradient spin echo (d-PGSE) sequence, shown in Fig. 1(a), is comprised of two diffusion sensitizing gradient pairs, $\mathbf{G_1}$ and $\mathbf{G_2}$ with durations of δ_1 and δ_2, respectively, that are separated by a mixing time (t_m). Note that in d-PFG two diffusion periods exist, Δ_1 and Δ_2, in which the spins are allowed to diffuse. The corresponding q values for each wave vector can be considered as $q=|\mathbf{q_1}|=|\mathbf{q_2}|$, where $\mathbf{q_i}=2\pi^{-1}\gamma\delta\mathbf{G_i}$. Another d-PFG sequence is shown in Fig. 1(b), in which t_m is effectively zero since the two inner gradients (the second $\mathbf{G_1}$ and the first $\mathbf{G_2}$) are superimposed. An important variant in the d-PFG methodology is the angle ψ between the gradient pairs [Fig. 1(c)]. In a recent study,[58] which theoretically studied the NMR signal decay due to diffusion in multiple-PFG experiments, rather peculiar phenomena were predicted, including zero-crossings of the signal decay for d-PFG experiments (negative diffusion-

diffractions). The zero-crossings were recently experimentally observed for the first time,[59] and the effect of the experimental parameters on these negative diffractions was studied. The d-PFG sequence was first theoretically studied by Mitra in 1995 in the low-q regime and in limiting cases of the gradient durations, the diffusion periods, and mixing times.[60] Mitra's study predicted that when the angle ψ between the gradient pairs is varied, an angular dependence of the signal decay for q values that fulfill $2\pi qa < 1$ occurs, (where "a" is the dimension of monodisperse pores), arising from microscopic anisotropy imposed by the boundaries of the restricting compartment. Mitra's limiting cases were recently theoretically extended to account for all of the d-PFG variables, including, cases of violating the short gradient pulse (SGP) condition, and for all gradient orientations, diffusion periods and mixing times.[61] The theoretical predictions were verified experimentally on well-controlled systems, in which the ground-truth is known *a priori*.[62] In another recent study, the theory was extended to any value of $2\pi qa$, enabling extraction of structural information for virtually any value of q.[63] The crucial finding of the above theoretical and experimental studies is that accurate compartment sizes can be extracted at wave vectors which are much smaller than the reciprocal of the pore dimension. This methodology obviates the need to reach high q-values which are needed to take advantage of the s-PFG diffusion-diffraction measurements. The direct implication is that even very small pores can be probed at relatively low q-values, which may be clinically feasible. Moreover, a very recent theoretical study predicts the ability of d-PFG to differentiate between different compartmental shapes due to sensitivity of d-PFG to compartment shape anisotropy (CSA), an intractable property for the s-PFG methodology.[64] Another recent study dealt with the effect of adding a free diffusion compartment to the microcapillaries, thus creating a superposition of free and restricted diffusion modes, which is characteristic of many real life systems.[65] In fact, in Ref. 65, a loss of the angular dependence at the low-q regime was observed due to masking of the free diffusion component. Several other groups have also exploited the angular dependence using Mitra's theory to extract structural information[66–68] in the low-q regime.

In this study, we employ the theory initially presented in Refs. 58, 61, and 63, which predicts advantages in using d-PFG experiments to explicitly study the properties of the signal decay in single- and double-PFG experiments with respect to size distributions in settings that are relevant to porous media. We study the possibility of d-PFG to extract structural information, which surpasses the information obtained from s-PFG, and the effect of variation in the experimental parameters. We then sought to experimentally verify the theoretical predictions in well-controlled phantoms, consisting of water-filled microcapillaries, in which the ground-truth, i.e., the size distribution and orientation of the pores, is known *a priori*. We show the gradual loss of diffusion-diffraction in increasingly disperse pore sizes in s-PFG experiments, and that the d-PFG retains both a robust zero-crossing (negative diffraction) and a signature for the width of the distribution, thus enabling extraction of structural information from the sample.

II. MATERIALS AND METHODS

A. Theory

In a double-PFG experiment with infinitesimally narrow diffusion gradients, the NMR signal attenuation for a single pore can be written to be [for the sequence shown in Fig. 1(a)]

$$\begin{aligned} \mathrm{E}^{A}_{\Delta_1,\mathrm{t_m},\Delta_2}(\mathbf{q_1},\mathbf{q_2}) &= \int d\mathbf{r_1}\rho(\mathbf{r_1})e^{-i2\pi\mathbf{q_1}\cdot\mathbf{r_1}}\int d\mathbf{r_1'}P_{\Delta_1}(\mathbf{r_1},\mathbf{r_1'})e^{i2\pi\mathbf{q_1}\cdot\mathbf{r_1'}} \\ &\times\int d\mathbf{r}_2P_{t_m}(\mathbf{r_1'},\mathbf{r}_2)e^{i2\pi\mathbf{q_2}\cdot\mathbf{r_2}}\int d\mathbf{r_2'}P_{\Delta_2}(\mathbf{r_2},\mathbf{r_2'})e^{-i2\pi\mathbf{q_2}\cdot\mathbf{r_2'}}, \end{aligned} \tag{2}$$

where $\rho(\mathbf{r})$ is equal to the reciprocal of the pore volume within the pore space, and zero elsewhere, and $P_\tau(\mathbf{r},\mathbf{r}')$ indicates the probability for a spin located at $\mathbf{r}$ to travel to $\mathbf{r}'$ after a time τ (in this case Δ_1, Δ_2, or $\mathrm{t_m}$). The above equation is valid for the pulse sequence of Fig. 1(a). As the mixing time approaches 0 the pulse sequence shown in Fig. 1(b) is achieved. The corresponding expression for the NMR signal intensity is given for the sequence shown in Fig. 1(b) by

$$\begin{aligned} \mathrm{E}^{B}_{\Delta_1,0,\Delta_2}(\mathbf{q_1},\mathbf{q_2}) &= \int d\mathbf{r_1}\rho(\mathbf{r_1})e^{-i2\pi\mathbf{q_1}\cdot\mathbf{r_1}}\int d\mathbf{r_1'}P_{\Delta_1}(\mathbf{r_1},\mathbf{r_1'})e^{i2\pi(\mathbf{q_1}+\mathbf{q_2})\cdot\mathbf{r_1'}} \\ &\times\int d\mathbf{r_2'}P_{\Delta_2}(\mathbf{r_1},\mathbf{r_2'})e^{-i2\pi\mathbf{q_2}\cdot\mathbf{r_2'}}, \end{aligned} \tag{3}$$

where we have employed the relationship $\lim_{\tau\to 0}P_\tau(\mathbf{r},\mathbf{r}') = \delta(\mathbf{r}-\mathbf{r}')$.

It is instructive to consider the limiting case of $\Delta_1=\Delta_2 \to\infty$. Because of the relation $\lim_{\tau\to\infty}P_\tau(\mathbf{r},\mathbf{r}')=\rho(\mathbf{r}')$ it is clear that in the long diffusion time limit, the above equation becomes

$$\mathrm{E}^{B}_{\infty,0,\infty}(\mathbf{q_1},\mathbf{q_2}) = \tilde{\rho}(\mathbf{q_1})\tilde{\rho}(\mathbf{q_2})\tilde{\rho}(\mathbf{q_1}+\mathbf{q_2})^*, \tag{4}$$

where

$$\tilde{\rho}(\mathbf{q}) = \int d\mathbf{r}\rho(\mathbf{q})e^{-i2\pi\mathbf{q}\cdot\mathbf{r}}. \tag{5}$$

For a cylinder of radius R, if the gradient is applied perpendicular to the axis of the cylinder, the above integral yields

$$\tilde{\rho}(\mathrm{q}) = \frac{J_1(2\pi\mathrm{qR})}{\pi\mathrm{qR}}. \tag{6}$$

It should be noted that the single-PFG experiment is just a special case of the double-PFG acquisition where the corresponding signal intensity can be obtained by setting $\mathbf{q_1}=0$ in Eq. (4) to yield $\mathrm{E}^{\text{s-PFG}}_{\infty}(\mathbf{q})=|\tilde{\rho}(\mathbf{q})|^2$. Therefore, the s-PFG signal is always positive and vanishes when 2πqR takes the value of a zero of the first order Bessel function. This is the basis for the nonmonotonicity of the single-PFG MR signal.

The double-PFG signal, however, behaves differently at short mixing times. To illustrate this point, we shall revisit Eq. (4) and set $\mathbf{q_1}=\mathbf{q_2}=\mathbf{q}$. In this case, the signal intensity is

$$E^{B}_{\infty,0,\infty}(\mathbf{q},\mathbf{q}) = \tilde{\rho}(\mathbf{q})^2\tilde{\rho}(2\mathbf{q})^*.$$

Clearly, this finding suggests that when 4πqR takes the value of a zero of the first order Bessel function, i.e., at half the q-value at which the single-PFG signal minima is encountered, the MR signal intensity vanishes. However, since this form of the signal does not have to be positive, the signal goes through the horizontal axis into negative values, leading to zero-crossings, rather than rebounding from the horizontal axis.

As demonstrated in Ref. 58, unlike the minima of the single-PFG signal decay, the zero-crossings in the double-PFG acquisitions are expected to be robust to the heterogeneities in the specimen. For the behavior of the signal decay in double-PFG experiments with arbitrary timing parameters and for other geometries, the theory in Refs. 58 and 61 can be employed. For ensembles of ellipsoids and capped cylinders, where the pore orientations are allowed to be incoherent or randomly oriented, see the discussion in Ref. 64.

B. Simulations of the effect of broadening size distributions on the diffusion-diffraction patterns in single- and double-PFG

In these simulations, single- and double-PGSE experiments were simulated using the theory above for gradually broadening lognormal distribution of cylinders. Simulations were also computed for monodisperse cylinders. The size distribution profiles can be seen in Fig. 2(a). For each of these size distributions, E(q) profiles were computed for the sequence shown in Fig. 1(b), assuming that the SGP approximation is fulfilled, $\delta \rightarrow 0$, and in the long diffusion time regime ($D\Delta \gg R^2_{max}$), where R_{max} is the maximum radius found in the population of cylinders. For varying t_m, simulations were computed for the sequence shown in Fig. 1(a).

C. Experiments on size distribution phantoms

All measurements were performed on a Bruker 8.4 T NMR spectrometer equipped with a micro5 microimaging accessory capable of producing up to 190 G/cm along the x-, y-, and z-directions. Hollow microcapillaries with inner diameters (ID) of 10 ± 1, 13 ± 1, 17 ± 1, 19 ± 1, 20 ± 1, 21 ± 1, or 29 ± 1 μm (Polymicro Technologies, Phoenix, AZ, USA) were immersed in water for several days, prior to each experiment. Three different size distribution samples were prepared, namely, SD001, SD002, and SD003 [see Fig. 5(a) and Table I], which exhibited both a shift in average diameter and a gradually broadening width. The volumetric and numerical ratio for the three size distribution phantoms are presented in Table I. The microcapillaries were carefully counted to comprise the accurate ratio of fibers needed in each sample. The microcapillaries were then cut to the same length, and packed into a 4 mm glass sleeve which was inserted into a 5 mm NMR tube. The 5 mm NMR tube was aligned with the main axis parallel to the z-direction of the magnet [Fig. 1(d)]. Typical line widths of 4–20 Hz were obtained after shimming for all size distribution phantoms.

D. Single- and double-PGSE experiments on the size distribution phantoms

The s-PFG experiments were conducted on the three size distribution phantoms SD001, SD002, and SD003, as well as on a sample of monodisperse microcapillaries with ID $=19\pm1$ μm. The experiments were all performed with the following parameters: 48 q-values were collected with G_{max} of 160 G/cm and with $\Delta/\delta=150/3$ ms, resulting in a q_{max} of 2043 cm^{-1} and with number of scans (NS) of 32.

The corresponding d-PFG experiment was performed on the same phantoms with the sequence shown in Fig. 1(b), and with the following parameters: both gradient pairs were in the x-direction (i.e., $\psi=0°$); 48 q-values were collected with $G_{1\,max}=G_{2\,max}=80$ G/cm and with $\delta_1=\delta_2=\delta_3=3$ ms, resulting in a q_{max} of 1021.5 cm^{-1} and with diffusion times $\Delta_1=\Delta_2=150$ ms and with NS=64. The results in all of the d-PFG experimental plots are presented as a function of 2q to be comparable with the s-PFG results.[59,65]

To test the effect of the mixing time, the phantom with the largest standard deviation was used, namely, SD003. The experiments were performed with the same experimental parameters as above, except that for t_m of 6, 25, and 50 ms, the sequence shown in Fig. 1(a) was used.

To test the effect of the size distributions on the angular dependence, the monodisperse 19 ± 1 μm microcapillaries and SD003 were used. Eight q-values were collected with $\delta_1=\delta_2=\delta_3=3$ ms and $G_{1\,max}=G_{2\,max}=80$ G/cm leading to a maximum q-value of 1021 cm^{-1}, and with $\Delta_1=\Delta_2=150$ ms using the sequence shown in Fig. 1(b). In this set of experiments, $\mathbf{G_1}$ was fixed in the x-direction, and the angle ψ between the gradients was varied with $\theta=90°$ (i.e., the orientation of $\mathbf{G_2}$ was varied in the X-Y plane [Fig. 1(e)], for a detailed explanation of such experiments, see Refs. 61, 62, and 65). The number of scans was set to 16.

III. RESULTS

A. Simulations of the effect of broadening size distributions on the diffusion-diffraction patterns in single- and double-PFG.

The size distributions used in the theoretical part of this study are shown in Fig. 2(a). We used a lognormal distribution of cylinders with a mean pore radius (R_0) of 4 μm and with cylindrical geometry. The standard deviation of the distribution was varied between $\sigma/R_0=0$ (monodisperse pores) and $\sigma/R_0=0.8$.

Figure 2(b) shows the theoretical plot of the NMR signal decay in s-PFG experiments satisfying the SGP approximation for increasing standard deviation of the size distribution. For monodisperse pores, the deep diffusion-diffraction troughs can be clearly seen with the first dip occurring at q $=1526$ cm^{-1}, corresponding to a compartment size of 8 μm. Increasing the standard deviation of the sample to a very modest value of $\sigma/R_0=0.05$ has already a profound effect on the diffusion-diffraction patterns. The diffusion-diffractions troughs are shallower and broader with the diffraction mini-

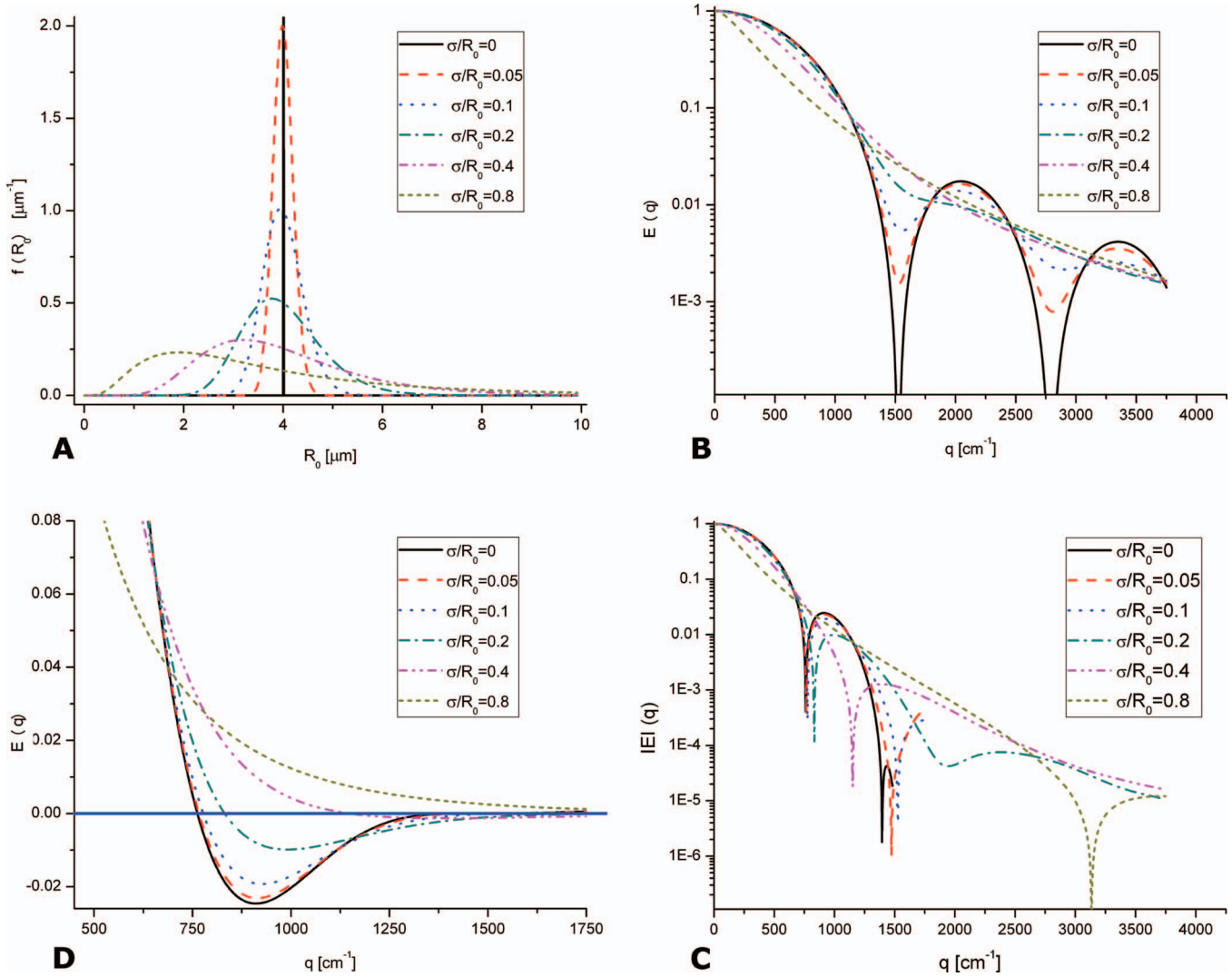

FIG. 2. Simulations of single and double-PFG signal decay for cylindrical pores characterized by size distributions. (a) The lognormal size distributions used for the simulations. Note that the size distributions were characterized by the mean radius, $R_0=4$ μm with increasing σ/R_0 values. The peak of the distribution moves towards smaller sizes with increasing σ/R_0 values to compensate for the fattening tail of the distribution. (b) Simulation of E(q) plots for s-PFG experiments for each size distribution shown in (a). The simulations were carried out under a fulfilled SGP condition, i.e., $\delta \ll R_0^2/D$, and in the long diffusion period regime, i.e., $\Delta \gg R_0^2/D$ for the direction perpendicular to the main axis of the microcapillaries. Note the rapid loss of diffusion-diffraction troughs with increasing σ/R_0. (c) Simulation of the magnitude calculated signal decay, $|E(q)|$, for d-PFG experiments for each size distribution shown in (a). The same conditions were used as in (b) for the sequence shown in Fig. 1(b) with $\Delta=\Delta_1=\Delta_2$ and $\delta=\delta_1=\delta_2=\delta_3$, and with $\psi=0°$ (both gradients were in the x-direction). The diffusion-diffraction troughs are readily observed for each of the size distributions. The location of the first diffusion-diffraction troughs in d-PFG experiments occurs at half of the q-value of that in s-PFG experiments and the q-value of the diffusion-diffraction dip is shifted to higher q-values as σ/R_0 is increased. For $\sigma/R_0=0$, 0.05 and 0.1, the plot is only partially shown, for convenience. (d) Real (not magnitude calculated) plots for the d-PFG simulations, shown for a partial range of q-values. Note that the signal minimum becomes higher with increasing σ/R_0, and that the rate of return of the signal to zero is slower with increasing σ/R_0. Note that the d-PFG signal decay is plotted as function of 2q to enable easy comparison with s-PFG.

TABLE I. Numerical ratio (left) and normalized volumetric ratio (right) of the experimental size distribution phantoms.

Nominal diameter (μm)	Numerical ratio			Normalized volumetric ratio		
	SD001	SD002	SD003	SD001	SD002	SD003
10 ± 1	0	10	10	0	0.078	0.129
13 ± 1	1	9	8	0.028	0.118	0.174
17 ± 1	3	10	5	0.142	0.224	0.187
19 ± 1	6	11	5	0.356	0.308	0.232
20 ± 1	5	0	0	0.329	0	0
21 ± 1	2	6	3	0.145	0.205	0.170
29 ± 1	0	1	1	0	0.065	0.108

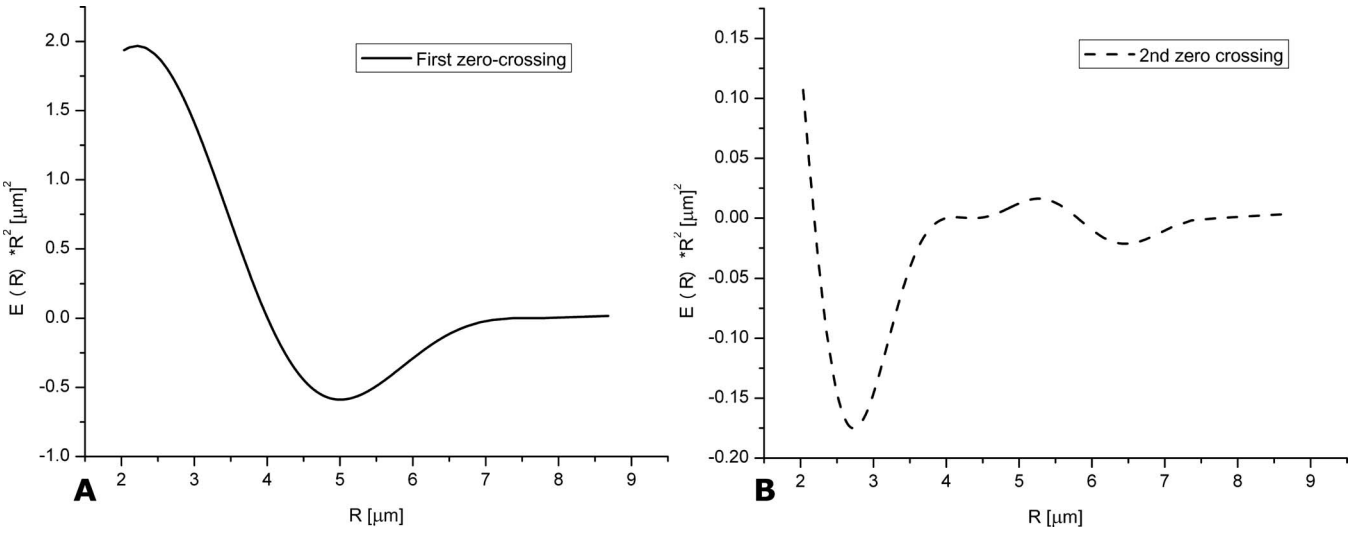

FIG. 3. Contribution of each pore present in the size distribution with $\sigma/R_0=0.2$ to the NMR signal. (a) The signal contributed from each pore at q $=1522\ cm^{-1}$ (the q-value at which the first zero-crossing is expected for a single cylinder of radius $R_0=4\ \mu m$ is expected) and (b) at $q=2790\ cm^{-1}$ (the q-value at which the second zero-crossing is expected for a single cylinder of radius $R_0=4\ \mu m$ is expected). Note that the signal is multiplied by R^2 to normalize for the number of spins in each pore.

mum remaining around $q=1530\ cm^{-1}$. As σ/R_0 is further increased to 0.1, the diffusion-diffraction trough becomes even shallower and wider. When $\sigma/R_0=0.2$, the diffusion-diffraction minimum is almost completely lost, and the signal decay loses its nonmonotonicity. At this point, the structural features, including the indication for restricted diffusion taking place, are almost completely lost. The wider the size distribution becomes, the smoother the signal decay in s-PFG experiments; for $\sigma/R_0=0.4$ and 0.8 it is impossible to obtain structural information directly from the signal decay [Fig. 2(b)].

Simulations of the signal decay in d-PFG experiments satisfying the SGP approximation and with $t_m=0$ ms are shown in Figs. 2(c) and 2(d). The magnitude calculated curve is shown in Fig. 2(c) to show the diffusion-diffraction patterns, while parts of the real curve are shown in Fig. 2(d) to show the actual zero-crossing of the signal.

The most striking effect that can be seen in Fig. 2(c) is that regardless of the ratio of σ/R_0 used, clear, sharp diffusion-diffraction troughs can be observed. For $\sigma/R_0=0$ the curve is shown only up to $q=1480\ cm^{-1}$, and for $\sigma/R_0=0.05$ and 0.1, the curve is shown only up to $q=1750\ cm^{-1}$ for clarity. As depicted in Fig. 2(c), the position of the first diffusion-diffraction troughs for $\sigma/R_0=0$, 0.05, 0.1, 0.2, 0.4, and 0.8 are 763, 765, 776, 832, 1151, and 3135 cm^{-1}, respectively. Note that although the first zero-crossing is well preserved in all of the simulations, the second diffusion-diffraction trough for $\sigma/R_0=0.2$ is shallow and broad and somewhat resembles the s-PFG wide dips observed in this particular distribution. As σ/R_0 increases, the q-value of the first diffusion-diffraction trough in the d-PFG simulations shifts towards higher q-values while the peak of the distribution shifts towards smaller sizes.

The actual zero-crossings of the signal decay in the d-PFG simulations can be seen in Fig. 2(d). Note that the rate of return of the signal to zero value qualitatively carries a signature for σ/R_0. The wider the distribution, the more slowly the signal returns to 0. For $\sigma/R_0<0.2$, a second zero-crossing exists: this time the signal crosses again from negative to positive values. However, for $\sigma/R_0>0.2$, only the first zero-crossing persists, and the signal remains negative with increasing q-values. Therefore, as the width of the distribution becomes larger, the return of the signal in the d-PFG plot towards zero is slower.

The underlying reason for the persistence of only the first zero-crossing in d-PFG can be realized from inspecting the signal intensity contributed from each cylinder in a size distribution at q-values corresponding to the zero-crossings of the signal. Figures 3(a) and 3(b) show the $E(R)^*R^2$ plots for the first and second zero-crossing, respectively, for the size distribution characterized by $\sigma/R_0=0.2$. The signal intensity E(R) is multiplied by R^2 to normalize for the number of spins diffusing in each pore. At the q-value that corresponds to a zero-crossing, there are spins that contribute negative signal while others contribute positive signal. At the *q*-value in which the first zero-crossing is expected for a single cylinder, [Fig. 3(a)], the contribution of negative and positive signal is equal, leading to the zero value of the signal. However, at the q-value in which the second zero-crossing is expected for a single cylinder of $R_0=4\ \mu m$ the contribution of negative signal from smaller pores is clearly larger. Therefore, the signal remains consistently negative for larger σ/R_0, while the first zero-crossing persists.

Simulations of the effect of prolonging t_m on the signal decay in d-PFG experiments are shown in Fig. 4(a). The curves are plotted for the size distribution in which $\sigma/R_0=0.2$, the value at which the s-PFG begins to lose the diffusion-diffraction dips. As described above, when $t_m=0$ ms, and the magnitude calculated curves are plotted against the q-values, the first diffusion-diffraction trough, originating from the zero-crossing of the signal, is observed at $q=832\ cm^{-1}$ [Fig. 2(c), Fig. 4(a)]. When t_m is prolonged to 1 and 2 ms, the location of the trough dramatically shifts towards higher q-values to $q=975$ and $1406\ cm^{-1}$, respec-

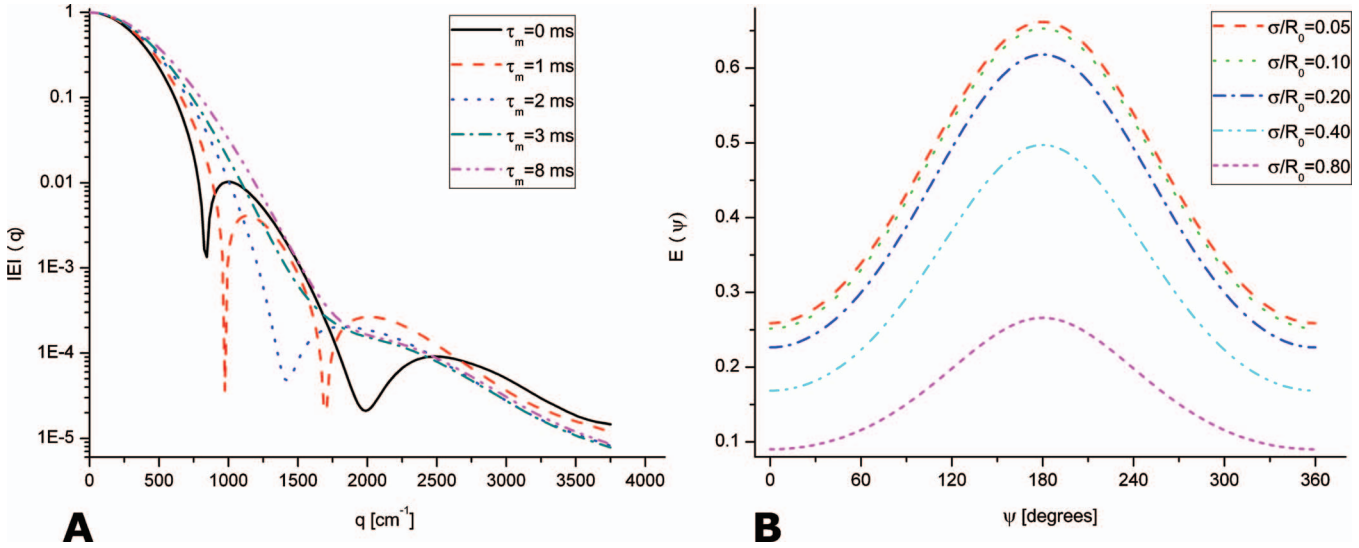

FIG. 4. Mixing time dependence and angular dependence in d-PFG simulations of size distribution specimens. (a) Dependence of the magnitude calculated signal decay, $|E(q)|$ on the mixing time. The diffusion-diffraction patterns are quickly lost when t_m is increased. (b) Simulation of the $E(\psi)$ angular dependence in d-PFG experiments for $q=500\ cm^{-1}$ for the different size distributions, carried out with the conditions mentioned in Fig. 2. Note that $\mathbf{G}_1$ was set in the x-direction and $\theta=90°$, i.e., the orientation of $\mathbf{G}_2$ was varied in the X-Y plane [as shown in Fig. 1(e)].

tively. Further prolongation of t_m to only 8 ms results in a complete loss of the diffusion-diffraction trough and loss of the structural information characterizing the pores [Fig. 4(a)].

Figure 4(b) shows the $E(\psi)$ simulations for the d-PFG conducted on an ensemble of cylinders with a mean radius of 4 μm. The angle ψ between the gradients was varied with $\theta=90°$, i.e., in the X-Y plane. The simulations were computed for increasing σ/R_0 and for $q=500\ cm^{-1}$, under conditions of fulfilled SGP condition and in the long diffusion time limit. The angular dependence, which arises from microscopic anisotropy (μA),[61,63] can be observed in all of the curves. Note that for $\psi=0°$ and the gradients in the x-direction, the value of $E(\psi)$ reduces to the values shown in Fig. 2(c) for the different σ/R_0 values at $q=500\ cm^{-1}$; this is why each curve begins at a different signal value. Nevertheless, as shown in Fig. 4(b), the angular dependence seems to be a robust property that does not change significantly with the width of the size distribution.

B. Single- and double-PGSE experiments on size distribution phantoms

After establishing that the diffusion measurements are indeed in the long diffusion time regime (data not shown, see Refs. 31, 32, and 59), single- and double-PGSE experiments were performed on the monodisperse phantom and on the size distribution phantoms SD001, SD002, and SD003. The normalized volumetric ratios of sizes present in the size-distribution phantoms are shown in Fig. 5(a) and summarized in Table I. The average diameters and standard deviations for SD001, SD002, and SD003 are 18.8 ± 1.9, 16.0 ± 4.3, and 14.9 ± 4.6 μm, respectively. As a comparison for the σ/R_0 measure (which characterizes real, continuous distributions) which was presented in the simulations, we computed the σ/R_{av} ratio for the discrete size distribution phantoms, which are $\sigma/R_{av}=0.10$, 0.27, and 0.31 for SD001, SD002, and SD003, respectively.

The experimental signal decay from s-PFG experiments on the size distribution phantoms is shown in Fig. 5(b). The monodisperse microcapillaries yielded well resolved, deep diffusion-diffraction troughs with the first minimum observed at $q=638\ cm^{-1}$, corresponding to a compartment size of 19.1 μm. However the E(q) profile changes dramatically when the measurements were performed on the SD001 phantom. Although SD001 was designed to have only a slight variation of diameters ($\sigma/R_{av}=0.10$), the diffusion-diffraction troughs in s-PFG become profoundly shallower, yielding wider minima which are nevertheless still observable at $q\sim680\ cm^{-1}$. When SD002 and SD003 are used ($\sigma/R_{av}=0.27$ and 0.31, respectively), the sharp diffusion-diffraction minima are almost completely lost, and it is impossible to use the E(q) data to obtain microstructural information characterizing the phantoms. A "bump" in the signal decay can be observed at $q\sim1150\ cm^{-1}$ for SD003, which may reflect a very shallow diffusion-diffraction dip, but from which accurate structural information cannot be obtained.

Examining the $|E(q)|$ plots for the d-PGSE experiments performed on these phantoms reveals a completely different picture [Fig. 5(c)]. Here, the diffusion-diffraction minima are sharp and present for all of the size distribution phantoms used (the data were magnitude calculated to reveal the diffusion-diffraction patterns, and the data are plotted as a function of 2q to be comparable to the s-PFG data). The location of the first minima for 19 ± 1 μm (monodisperse), SD001, SD002, and SD003 are observed at $q=638$, 680, 808, and 936 cm^{-1}, respectively, and correspond to diameters of 19.1, 17.9, 15.1, and 13.0 μm, respectively. These sizes are in good agreement with the average diameters of

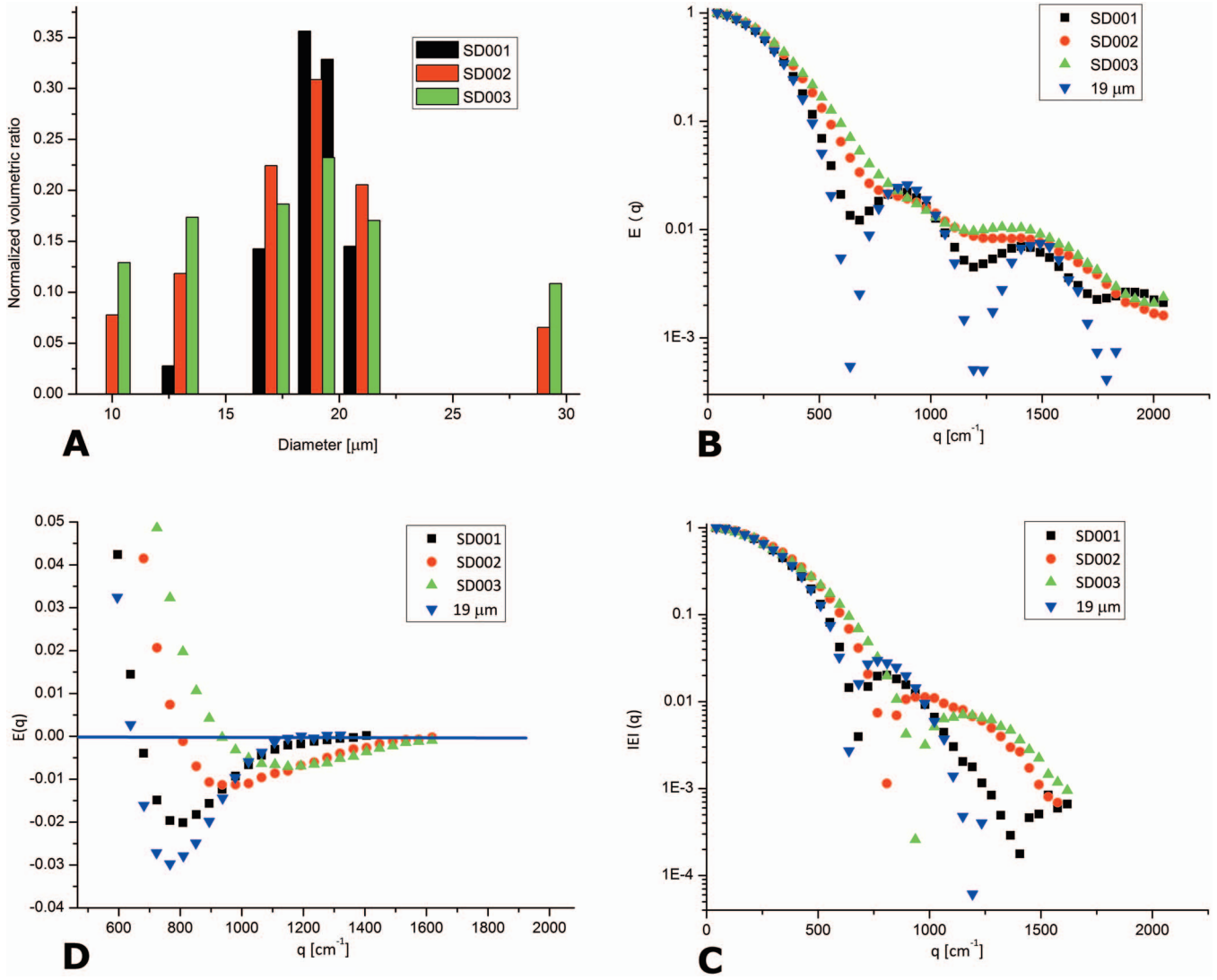

FIG. 5. Experimental study of single- and double-PFG methodologies in size distribution phantoms. (a) The volumetric ratio of sizes present in each size distribution phantom. (b) E(q) plots of s-PFG experiments for a monodisperse phantom and for SD001-SD003 shown in (a). The s-PFG experiments were carried out with $\Delta/\delta=150/3$ ms in the long diffusion regime. Note the gradual loss in diffusion-diffraction troughs. (c) The magnitude calculated signal decay $|E(q)|$ of d-PFG experiments for the phantoms. In these experiments, comparable to the s-PFG experiments, $\Delta_1=\Delta_2=150$ ms and $\delta_1=\delta_2=\delta_3=3$ ms were used with the sequence shown in Fig. 1(b). The data are plotted as a function of 2q to enable easy comparison to s-PFG data. Note that the diffusion-diffraction patterns are easily observed; the location of the diffusion-diffraction minima shifts towards higher q-values between SD001 and SD003. (d) The real (not magnitude calculated) signal decay, E(q), for the d-PFG experiments, shown for a partial range of q-values. The signal minimum increases with increasing σ/R_{av} and the rate of return of the signal to zero is slower for increasing values of σ/R_{av}.

the size distribution phantoms with a slight deviation towards smaller sizes, most likely due to a slight violation of the SGP approximation.

Figure 5(d) shows the real signal decay, E(q), without the magnitude calculation, for d-PFG experiments on the monodisperse and size distribution phantoms. From these plots, one may observe several phenomena. First, as pointed out above, the location of the diffusion-diffraction minima is manifested as an actual zero-crossing of the signal. Second, the q-value in which a minimum point of the plot is achieved becomes higher with increasing width of distribution. Finally, the rate of return of the signal to noise level in the negative part also depends strongly on the width of the distribution (a manifestation of the lack of a second diffusion-diffraction trough in the magnitude calculated plots). The wider the distribution, the more slowly the signal returns to noise level.

The dependence of the zero-crossings on the mixing time is shown in Fig. 6(a) for SD003. Even for the shortest nonzero t_m possible using our gradient system (considering the gradient duration and eddy currents), namely, $t_m=6$ ms, the diffusion-diffraction minimum is lost in the d-PFG plot. Further prolonging the mixing time to 25 ms results in a slower attenuation rate; prolonging the mixing time to 50 ms reveals a similar signal decay.

The angular dependence $E(\psi)$ is shown in Fig. 6(b) with $\mathbf{G_1}$ fixed along the x-direction and $\theta=90°$, i.e., the angle ψ between the gradients was varied in the X-Y plane. Figure 6(b) shows the signal decay for $q=329$ and 467 cm^{-1} for monodisperse 19 ± 1 μm microcapillaries and for the size distribution phantom SD003. Here, the angular dependence can be clearly seen for both size distribution phantoms, and for both q-values. Despite the large difference in σ/R_{av}, the

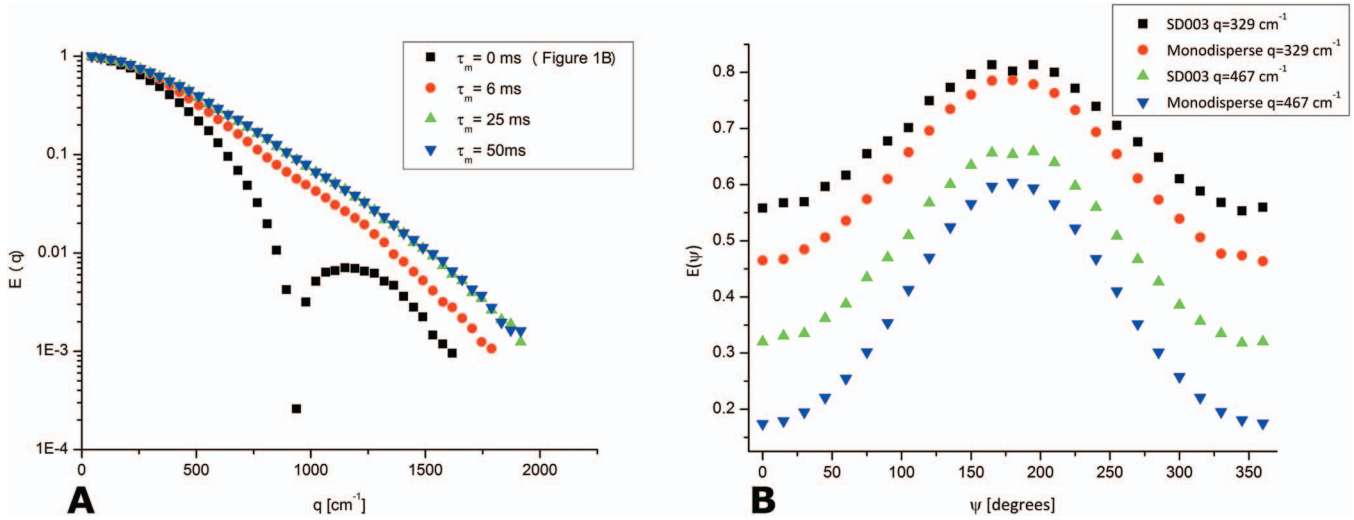

FIG. 6. Experimental study of the mixing time dependence and the angular dependence in the size distribution phantoms. (a) The mixing time dependence for SD003, note that the magnitude calculated signal decay, $|E(q)|$ is shown. The same parameters were used as mentioned in Fig. 5, but for $t_m=6$, 25, and 50 ms the sequence shown in Fig. 1(a) was used. Note the rapid loss of the diffusion-diffraction patterns when the mixing time is prolonged. (b) The angular dependence $E(\psi)$ for the monodisperse 19 ± 1 μm microcapillaries and for SD003 at two different q-values. Note that $\mathbf{G}_1$ was set in the x-direction and $\theta=90°$, i.e., the orientation of $\mathbf{G}_2$ was varied in the X-Y plane [Fig. 1(e)]. In both cases, the diffusion periods were sufficiently long to probe the boundaries of the restricting compartment.

angular dependence for both phantoms persists from which one can infer the presence of restricted diffusion.

IV. DISCUSSION

Inferring microstructural information such as pore size, orientation, and shape is extremely important for accurately characterizing porous media in a wide range of applications. Therefore, developing methodologies that would enable an accurate portrayal of such microstructural features is of paramount importance. Indeed, diffusion NMR is an extremely important tool for such applications. When restricted diffusion occurs, it may provide an excellent means of probing the confining geometries, owing to the sensitivity of the extracted ADC towards the imposed barriers.[1,3,12,27]

In homogenous, monodisperse pores, the diffusion-diffraction patterns that are observed in the NMR signal decay are a manifestation of restricted diffusion. These patterns have been shown to be extremely useful in characterizing both the size of the compartment and the orientation of the pores: the location of diffusion-diffraction troughs are excellent reporters for compartment size,[28,31,32,69] and it has been shown that the diffraction troughs can be observed only when the gradients are applied very close to 90° (with respect to the main axis of the microcapillaries), thus providing excellent sensitivity for the orientation of the pores.[28] Moreover, the diffusion-diffraction troughs bear a signature for the occurrence of restricted diffusion in monodisperse pores, an important attribute that is not always easily inferred.

Many realistic systems including, for example, neuronal tissues are not characterized by monodisperse compartmental dimensions. When such systems are probed using s-PFG variants of diffusion NMR, the microstructural information, as extracted by the diffusion-diffraction troughs, is lost. In most cases, when the pores are characterized by a continuous size distribution, the signal decay is characterized by a featureless nonmonoexponential decay.[41,48] The q-space approach, which enables extraction of fast and slow components from the Fourier transform of the signal decay may provide an estimate towards the relative mean size of pores and their orientation due to accentuation of the slow component;[41,70] nevertheless, it does not provide estimates or signatures for the width of the size distributions. Properties of the size distributions may be extremely important to derive: in neuronal tissue, emulsions, rocks, and other applications, the size distribution may be of importance in characterizing the specimen in question.

In the present study, the loss of diffusion-diffraction patterns due to size distributions in s-PFG was revealed as an inherent property of the s-PFG methodology. We have been able to show that even for a modest size distribution, characterized by σ/R_0 of only 0.2, the diffusion-diffraction troughs almost completely disappear. It is noteworthy that although we chose a lognormal distribution of cylindrical pores, the same holds for other types of size distributions and for pores of different shapes (data not shown). The underlying reason for the loss of diffusion-diffraction troughs in s-PFG lies in the additive nature of the signal decay, which encompasses contributions from all pores present within the MR voxel. The reciprocal nature of the diffusion-diffraction trough and the pore size means that the smaller pores push the diffusion-diffraction troughs towards higher q-values, generating a slowly decaying signal, while the larger pores tend to push the diffusion-diffraction troughs towards lower q-values, generating a signal that attenuates more rapidly. Another determinant is the number of spins in each pore. The fractional sum of these contributions leads to a complete disappearance of the diffusion-diffraction troughs in s-PFG, and eventually to a featureless decay curve that resembles multiexponential decay.

On the contrary, the simulations for the d-PFG methodology reveal that sharp zero-crossings (which manifest as

diffusion-diffraction troughs in magnitude calculated plots) persist, regardless of the size distribution employed. It should be noted that although we only presented simulations with standard deviations of up to $\sigma/R_0=0.8$, the zero-crossings can be observed even for much larger values of σ/R_0. The underlying reason for the persistence of the first zero-crossing was also shown in this study, and was found to be due to cancellation of signal from small pores and signal from larger pores. This cancellation is also probably the reason why the location of the zero-crossing is closer to the position of the peak of the distribution than to R_0. Importantly, the loss of the second zero-crossing when σ/R_0 is increased leads to a fingerprint for the width of the distribution: for the broader distributions the signal will remain negative and will approach the abscissa more slowly, since the signal from neighboring pores does not cancel at the higher q-values.

We sought to experimentally validate these theoretical predictions on a well-characterized system, in which the ground-truth is known *a priori*. The very well-characterized system of water-filled microcapillaries of different sizes, which were counted in order to comprise different volumetric ratios of each size, served as a useful phantom for that purpose. In these phantoms, determinants such as the size of the individual components of the size distribution phantoms, as well as the volumetric contribution of each size, and the orientation of the pores are all very well defined. Moreover, diffusion in these microcapillaries has been extensively studied, and the response of the diffusion-diffraction patterns to variations in many experimental parameters has been shown for these microcapillaries in a number of studies.[28,31–33,59,62,63,65] The main advantages for such a phantom is that the ground-truth is known *a priori*, such that a controlled increase in width of the mixture is possible; moreover, in these microcapillaries, completely restricted diffusion can be achieved, without exchange or permeability of the restricting compartment. We found that the theoretical predictions that were first published in Refs. 58 and 61, which predicted that zero-crossings should persist in d-PFG even when the specimen is characterized by size distributions, and were further theoretically extended here, are accurately manifested in the signal decay of the size distribution phantoms.

The experimental data in this study show that s-PFG experiments indeed incur a loss of diffusion-diffraction patterns with larger σ/R_{av}, and that the broader the distribution, the shallower the diffusion-diffraction troughs. The d-PFG experiments, on the other hand, which were conducted on the same phantoms, revealed that the zero-crossings persist, and upon magnitude calculation, the diffusion-diffraction dips can be clearly observed. The location of the diffusion-diffraction troughs in these phantoms was somewhat indicative of the average diameter characterizing the phantoms, an important property which was lost in s-PFG experiments. We have also been able to qualitatively show that the return of the signal to zero after the minimum point of the real (not magnitude calculated) E(q) data are indeed indicative of the width of the distribution. We have also been able to show the signal decay trends that were predicted by the theoretical study with respect to the mixing time and in the angular dependences. It is clear that for such experiments, the sequence with $t_m=0$ ms is inherently more robust towards size distributions. Previously, we have shown both theoretically[58,63] and experimentally[59,63] that the first zero-crossing is very sensitive to mixing times (as opposed to the second diffusion-diffraction trough), due to loss of correlation between the information encoded in the first and second diffusion periods. When monodisperse pores are present, this manifests in a shift in the location of the zero-crossing towards higher q-values, which gradually progresses into a complete loss of the zero-crossing. In this study, this phenomenon seems to contribute much more strongly, incurring a loss of the zero-crossing even with very short mixing times, probably due to the more significant contribution of the smaller pores in such cases.

Although we have shown that the d-PFG experiment is much more robust towards size distributions, some experimental limitations arise for using the d-PFG in such phantoms. The main disadvantage is that when the size distribution becomes broader, the location of the diffusion-diffraction minimum in the $|E(q)|$ plot is shifted towards higher q-values, which will necessitate the use of very strong gradients. This is acceptable for *ex vivo* and material science specimens, but not for *in vivo* studies. Furthermore, the difference between the zero-crossing and the noise level is lower for broader distributions, a fact which will require high signal-to-noise ratio, which is usually time-consuming. However, it seems that due to the important structural features that can be obtained from d-PFG experiments, the efforts may be well worthwhile.

Another finding was that the $E(\psi)$ angular dependence, an important attribute of d-PFG that enables extracting microstructural information such as compartment dimensions using low gradient amplitudes, is robust even when broad size distributions are present. In this study, an ensemble of infinite cylinders which are characterized by an effectively infinite $L \gg R_0$ (where L is the length of the cylinder and R_0 is the cylinder radius), were investigated. In such specimens, the three mechanisms of anisotropy (μA, CSA, and EA) are present.[64] However, the angular dependence is expected to be preserved even for polydisperse spherical pores, in which only μA exists.[61] Note that s-PFG can be used to extract anisotropy arising from macroscopic boundaries even when the specimen is isotropic;[71] however, d-PFG can fill an important niche in characterizing randomly oriented microstructures in terms of μA and CSA.[64]

A limitation of this study is that we did not use a continuous size distribution specimen, as found naturally in realistic porous media. The phantoms were chosen because of the need to validate the theoretical findings in a well-characterized setting in which the ground-truth is known, and for which the correct experimental parameters can be chosen on the basis of prior knowledge regarding the effects of the experimental parameters on the signal decay. Although these phantoms may be regarded as a discrete delta functions distribution rather than continuous size distribution, they have been useful in validating the theoretical framework. Further studies on more realistic systems such as emulsions and cell

suspensions are needed to determine the feasibility of using d-PFG methodologies for accurately extracting the relevant microstructural information. Such experiments are being carried out and will be reported in due course. Finally, we would like to point out that although the main focus of this paper is on heterogeneities in the compartment size, the d-PFG zero-crossings are expected to be robust to other kinds of heterogeneities that may be prevalent in the specimen. For example in Ref. 64, it was predicted that in the case of elongated structures, such as capped cylinders and ellipsoids, a dispersion in the orientations of these otherwise identical compartments does not lead to the disappearance of the zero-crossings. In fact, according to the simulations therein, even when the pores are distributed completely randomly with no coherence in their orientation, the d-PFG zero-crossing is expected to be preserved.

V. CONCLUSIONS

We have studied the disappearance of diffusion-diffraction patterns in s-PFG and the preservation of zero-crossings in the d-PFG methodologies, and have shown that the d-PFG methodology may overcome the limitations inherent to s-PFG. We have experimentally shown the vanishing of diffusion-diffraction patterns when the s-PFG methodology is conducted on size distribution phantoms, consisting of a combination of water filled microcapillaries with varying average sizes and standard deviations; in contrast, we have shown the persistence of the zero-crossings in the d-PFG methodology in the same phantoms. A qualitative fingerprint for the width of the distribution, manifested in the rate of return of the signal to zero after the signal minimum occurs in d-PFG experiments was demonstrated for d-PFG experiments. The persistence of the diffusion-diffraction patterns in d-PFG gives hope that specimens characterized by size distributions such as emulsions or neuronal tissues could be better characterized using the d-PFG methodology, as compared to s-PFG experiments.

ACKNOWLEDGMENTS

P.J.B and E.Ö. were supported by the Intramural Research Program of the Eunice Kennedy Shriver National Institute of Child Health and Human Development.

[1] Y. Cohen and Y. Assaf, NMR Biomed. **15**, 516 (2002).
[2] K. I. Momot and P. W. Kuchel, Concepts Magn. Reson. **28A**, 249 (2006).
[3] P. N. Sen, J. Phys.: Condens. Matter **16**, S5213 (2004).
[4] Y. Q. Song, Magn. Reson. Imaging **21**, 207 (2003).
[5] Y. Q. Song, H. Cho, T. Hopper, A. E. Pomerantz, and P. Z. Sun, J. Chem. Phys. **128**, 052212 (2008).
[6] A. T. Watson and C. T. P. Chang, Prog. Nucl. Magn. Reson. Spectrosc. **31**, 343 (1997).
[7] Y. Cohen, L. Avram, and L. Frish, Angew. Chem., Int. Ed. **44**, 520 (2005).
[8] R. L. Kleinberg, W. E. Kenyon, and P. P. Mitra, J. Magn. Reson., Ser. A **108**, 206 (1994).
[9] P. J. Basser, J. Mattiello, and D. LeBihan, J. Magn. Reson., Ser. B **103**, 247 (1994).
[10] D. Le Bihan, J. F. Mangin, C. Poupon, C. A. Clark, S. Pappata, N. Molko, and H. Chabriat, J. Magn. Reson Imaging **13**, 534 (2001).
[11] L. L. Latour, P. P. Mitra, R. L. Kleinberg, and C. H. Sotak, J. Magn. Reson., Ser. A **101**, 342 (1993).
[12] P. N. Sen, Concepts Magn. Reson. **23A**, 1 (2004).
[13] E. Özarslan, P. J. Basser, T. M. Shepherd, P. E. Thelwall, B. C. Vemuri, and S. J. Blackband, J. Magn. Reson. **183**, 315 (2006).
[14] P. T. Callaghan and A. A. Khrapitchev, Magn. Reson. Imaging **19**, 301 (2001).
[15] A. A. Khrapitchev, S. Stapf, and P. T. Callaghan, Phys. Rev. E **66**, 051203 (2002).
[16] A. A. Khrapitchev and P. T. Callaghan, Phys. Fluids **15**, 2649 (2003).
[17] J. D. Seymour and P. T. Callaghan, J. Magn. Reson., Ser. A **122**, 90 (1996).
[18] P. N. Sen and S. Axelrod, J. Appl. Phys. **86**, 4548 (1999).
[19] Y. Q. Song, J. Magn. Reson. **143**, 397 (2000).
[20] Y. Q. Song, S. G. Ryu, and P. N. Sen, Nature (London) **406**, 178 (2000).
[21] L. M. Burcaw and P. T. Callaghan, J. Magn. Reson. **198**, 167 (2009).
[22] P. T. Callaghan, S. Godefroy, and B. N. Ryland, Magn. Reson. Imaging **21**, 243 (2003).
[23] D. G. Cory and A. N. Garroway, Magn. Reson. Med. **14**, 435 (1990).
[24] K. G. Hollingsworth and M. L. Johns, J. Colloid Interface Sci. **258**, 383 (2003).
[25] E. O. Stejskal and J. E. Tanner, J. Chem. Phys. **42**, 288 (1965).
[26] P. T. Callaghan, A. Coy, D. Macgowan, K. J. Packer, and F. O. Zelaya, Nature (London) **351**, 467 (1991).
[27] W. S. Price, Concepts Magn. Reson. **9**, 299 (1997).
[28] L. Avram, Y. Assaf, and Y. Cohen, J. Magn. Reson. **169**, 30 (2004).
[29] P. T. Callaghan, J. Magn. Reson., Ser. A **113**, 53 (1995).
[30] S. L. Codd and P. T. Callaghan, J. Magn. Reson. **137**, 358 (1999).
[31] L. Avram, E. Özarslan, Y. Assaf, A. Bar-Shir, Y. Cohen, and P. J. Basser, NMR Biomed. **21**, 888 (2008).
[32] A. Bar-Shir, L. Avram, E. Özarslan, P. J. Basser, and Y. Cohen, J. Magn. Reson. **194**, 230 (2008).
[33] A. Bar-Shir and Y. Cohen, Magn. Reson. Imaging **26**, 801 (2008).
[34] A. Caprihan, L. Z. Wang, and E. Fukushima, J. Magn. Reson., Ser. A **118**, 94 (1996).
[35] B. Hakansson, R. Pons, and O. Söderman, Magn. Reson. Imaging **16**, 643 (1998).
[36] C. Malmborg, D. Topgaard, and O. Söderman, J. Colloid Interface Sci. **263**, 270 (2003).
[37] P. W. Kuchel, A. Coy, and P. Stilbs, Magn. Reson. Med. **37**, 637 (1997).
[38] J. F. Kuntz, G. Trausch, P. Palmas, P. Mutzenhardt, and D. Canet, J. Chem. Phys. **126**, 134904 (2007).
[39] W. S. Price, P. Stilbs, and O. Söderman, J. Magn. Reson. **160**, 139 (2003).
[40] D. Topgaard and O. Söderman, Magn. Reson. Imaging **21**, 69 (2003).
[41] A. Bar-Shir and Y. Cohen, NMR Biomed. **21**, 165 (2008).
[42] H. H. Ong, A. C. Wright, S. L. Wehrli, A. Souza, E. D. Schwartz, S. N. Hwang, and F. W. Wehrli, Neuroimage **40**, 1619 (2008).
[43] L. Ambrosone, A. Ceglie, G. Colafemmina, and G. Palazzo, J. Chem. Phys. **107**, 10756 (1997).
[44] L. Ambrosone, S. Murgia, G. Cinelli, M. Monduzzi, and A. Ceglie, J. Phys. Chem. B **108**, 18472 (2004).
[45] G. J. W. Goudappel, J. P. M. van Duynhoven, and M. M. W. Mooren, J. Colloid Interface Sci. **239**, 535 (2001).
[46] F. Wolf, L. Hecht, H. P. Schuchmann, E. H. Hardy, and G. Guthausen, Eur. J. Lipid Sci. Technol. **111**, 730 (2009).
[47] G. Pages, D. Szekely, and P. W. Kuchel, J. Magn. Reson. Imaging **28**, 1409 (2008).
[48] Y. Assaf and Y. Cohen, J. Magn. Reson. **131**, 69 (1998).
[49] K. G. Hollingsworth, A. J. Sederman, C. Buckley, L. F. Gladden, and M. L. Johns, J. Colloid Interface Sci. **274**, 244 (2004).
[50] K. G. Hollingsworth and M. L. Johns, J. Magn. Reson. **176**, 71 (2005).
[51] D. G. Cory, A. N. Garroway, and J. B. Miller, Polym. Preprints. **31**, 149 (1990).
[52] P. T. Callaghan, S. L. Codd, and J. D. Seymour, Concepts Magn. Reson. **11**, 181 (1999).
[53] A. Jerschow and N. Muller, J. Magn. Reson. **125**, 372 (1997).
[54] P. Galvosas, Y. Qiao, M. Schonhoff, and P. T. Callaghan, Magn. Reson. Imaging **25**, 497 (2007).
[55] P. T. Callaghan and M. E. Komlosh, Magn. Reson. Chem. **40**, S15 (2002).
[56] M. E. Komlosh, F. Horkay, R. Z. Freldlin, U. Nevo, Y. Assaf, and P. J. Basser, J. Magn. Reson. **189**, 38 (2007).
[57] M. E. Komlosh, M. J. Lizak, F. Horkay, R. Z. Freidlin, and P. J. Basser, Magn. Reson. Med. **59**, 803 (2008).
[58] E. Özarslan and P. J. Basser, J. Magn. Reson. **188**, 285 (2007).
[59] N. Shemesh and Y. Cohen, J. Magn. Reson. **195**, 153 (2008).

[60] P. P. Mitra, Phys. Rev. B **51**, 15074 (1995).
[61] E. Özarslan and P. J. Basser, J. Chem. Phys. **128**, 154511 (2008).
[62] N. Shemesh, E. Özarslan, P. J. Basser, and Y. Cohen, J. Magn. Reson. **198**, 15 (2009).
[63] E. Özarslan, N. Shemesh, and P. J. Basser, J. Chem. Phys. **130**, 104702 (2009).
[64] E. Özarslan, J. Magn. Reson. **199**, 56 (2009).
[65] N. Shemesh, E. Özarslan, A. Bar-Shir, P. J. Basser, and Y. Cohen, J. Magn. Reson. **200**, 214 (2009).
[66] J. Finsterbusch and M. A. Koch, J. Magn. Reson. **195**, 23 (2008).
[67] M. A. Koch and J. Finsterbusch, Magn. Reson. Med. **60**, 90 (2008).
[68] T. Weber, C. H. Ziener, T. Kampf, V. Herold, W. R. Bauer, and P. M. Jakob, Magn. Reson. Med. **61**, 1001 (2009).
[69] P. T. Callaghan, Magn. Reson. Imaging **14**, 701 (1996).
[70] A. Bar-Shir and Y. Cohen, J. Magn. Reson. **190**, 33 (2008).
[71] E. Özarslan, U. Nevo, and P. J. Basser, Biophys. J. **94**, 2809 (2008).